NANO LETTERS

Letter

pubs.acs.org/NanoLett

Band Gap Engineering with Ultralarge Biaxial Strains in Suspended Monolayer MoS_2

David Lloyd,[†] Xinghui Liu,[‡] Jason W. Christopher,[§] Lauren Cantley,[†] Anubhav Wadehra,[∥] Brian L. Kim,[†] Bennett B. Goldberg,[§] Anna K. Swan,[⊥] and J. Scott Bunch*[,†,#]

[†]Department of Mechanical Engineering, Boston University, Boston, Massachusetts 02215 United States

[‡]Department of Mechanical Engineering, University of Colorado, Boulder, Colorado 80309 United States

[§]Department of Physics, Boston University, 590 Commonwealth Avenue, Boston, Massachusetts 02215, United States

[∥]Department of Materials and Metallurgy, PEC University of Technology, Chandigarh, India 160012

[⊥]Department of Electrical and Computer Engineering, Boston University, 590 Commonwealth Avenue, Boston, Massachusetts 02215, United States

[#]Division of Materials Science and Engineering, Boston University, Brookline, Massachusetts 02446 United States

Supporting Information

ABSTRACT: We demonstrate the continuous and reversible tuning of the optical band gap of suspended monolayer MoS_2 membranes by as much as 500 meV by applying very large biaxial strains. By using chemical vapor deposition (CVD) to grow crystals that are highly impermeable to gas, we are able to apply a pressure difference across suspended membranes to induce biaxial strains. We observe the effect of strain on the energy and intensity of the peaks in the photoluminescence (PL) spectrum and find a linear tuning rate of the optical band gap of 99 meV/%. This method is then used to study the PL spectra of bilayer and trilayer devices under strain and to find the shift rates and Grüneisen parameters of two Raman modes in monolayer MoS_2. Finally, we use this result to show that we can apply biaxial strains as large as 5.6% across micron-sized areas and report evidence for the strain tuning of higher level optical transitions.

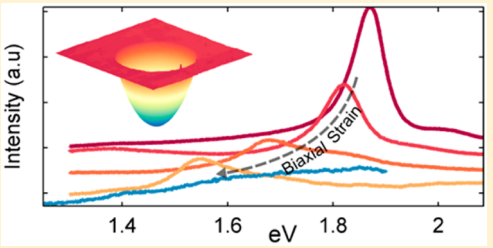

KEYWORDS: *Strain engineering, MoS_2, photoluminescence, bandgap, Raman spectroscopy, biaxial strain*

The ability to produce materials of truly nanoscale dimensions has revolutionized the potential for modulating or enhancing the physical properties of semiconductors by mechanical strain.[1] Strain engineering is routinely used in semiconductor manufacturing with essential electrical components such as the silicon transistor or quantum well laser using strain to improve efficiency and performance.[2,3] Nanostructured materials are particularly suited to this technique, as they are often able to remain elastic when subject to strains many times larger than their bulk counterparts can withstand.[4] For instance, bulk silicon fractures when strained to just 1.2%, whereas silicon nanowires can reach strains of as much as 3.5%.[5] Parameters such as the band gap energy or carrier mobility of a semiconductor, which are often crucial to the electronic or photonic device performance, can be highly sensitive to the application of only small strains. The combination of this sensitivity with the ultrahigh strains possible at the nanoscale could lead to an unprecedented ability to modify the electrical or photonic properties of materials in a continuous and reversible manner.

Monolayer MoS_2, a two-dimensional (2D) atomic crystal, has been shown in both theory[6,7] and experiment[8−12] to be an ideal candidate for strain engineering. It belongs to the class of 2D transition metal dichalcogonides (TMDs) and as a direct-gap semiconductor[13] has received significant interest as a channel material in transistors,[14] photovoltaics,[15] and photodetection[16] devices. It has a breaking strain of 6−11% as measured by nanoindentation, which approaches its maximum theoretical strain limit[17] and classifies it as an ultrastrength material. Its electronic structure has also proven to be highly sensitive to strain with experiments showing that the optical band gap reduces by ∼50 meV/% for uniaxial strain[8,11] and is predicted to reduce by ∼100 meV/% for biaxial strain.[18,19] This reversible modulation of the band gap could be used to make wavelength tunable phototransistors[16] or MoS_2 strain sensors that have a sensitivity comparable to their state of the art silicon counterparts.[20] Moreover, it has been suggested that strain could also improve the performance of MoS_2 transistors[21] or could be used to create broadband light absorbers for energy harvesting.[22]

The effect of strain on the band gap of 2D TMD's has been reported in a number of studies[9−12,20,23,24] including uniaxial strains of up to ∼4%[25] and biaxial strains of up to ∼3%

Received: June 24, 2016
Revised: August 1, 2016

DOI: 10.1021/acs.nanolett.6b02615
Nano Lett. XXXX, XXX, XXX−XXX

produced in highly localized submicron areas.[26] Band gap shifts in MoS_2 of ~300 meV have been induced by using very large hydrostatic pressures[27] and tensile strain has induced shifts of as much as ~100 meV.[11] However, the combination of being both an ultrastrength material and having a band gap highly sensitive to strain implies that a much larger band gap tuning must be possible. By contrast, tensile strain has been used to reduce the band gap by as much as 290 meV in 1D nanowires.[28]

In this paper, we use a geometry that allows us to take the first measurements of the Raman mode and band gap shift rates of suspended MoS_2 membranes under large biaxial strains and study single and multilayer samples prepared by both CVD and mechanical exfoliation. We conclude that micron scale CVD grown monolayer MoS_2 can be biaxially strained by over 5% resulting in an optical band gap reduction of ~500 meV or over 25%.

Our geometry exploits the fact that monolayer MoS_2, like graphene, is impermeable to all standard gases.[29] By applying a pressure difference across a MoS_2 membrane suspended over a cylindrical cavity (Figure 1a), a bulge is formed and this

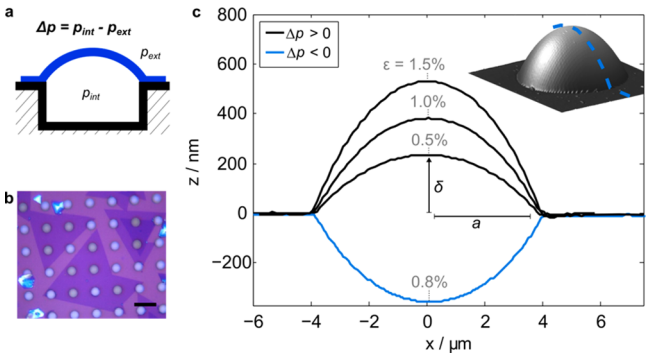

Figure 1. (a) Device schematic. (b) A typical sample of CVD grown MoS_2 membranes suspended over cylindrical cavities after transfer (scale bar is 20 μm). (c) An AFM cross section of a device at various p_{int}, resulting in different biaxial strains at the center of the device. Devices can be bulged up or down depending on whether Δp is positive or negative.

deformation produces a biaxial strain at the center of the device. To fabricate our devices, we first suspend MoS_2 films over cylindrical microcavities etched into a SiO_x/Si substrate by the transfer of CVD grown MoS_2 using a PMMA transfer method.[30] Figure 1b shows a typical transfer with a high yield of undamaged suspended devices. We used a novel CVD growth recipe (see Supporting Information for details) that produces highly impermeable monolayer membranes. With our best growths, a single transfer can produce several hundred suspended monolayer devices that are impermeable to the larger gas species (Figure S3).

Figure 1c shows atomic force microscopy (AFM) cross sections of one of these devices under ambient external pressures ($p_{ext} = p_{atm}$) but with increasing internal pressures (p_{int}), resulting in increasing center membrane deflections δ. The device can be bulged up ($\delta > 0$) or down ($\delta < 0$) depending on whether the pressure difference across the membrane, $\Delta p = p_{int} - p_{ext}$, is positive or negative. We vary p_{int} by placing the devices in a chamber filled with pressurized N_2 gas, which is able to slowly diffuse through the silicon oxide substrate and into the sealed microcavities. They are left there for several days until p_{int} equilibrates with the pressure of the N_2 gas.[29] After the devices are removed from the chamber, the new p_{int} results in a different δ and biaxial strain ε in the center of the device.

Following Hencky's model for circular, pressurized membranes with a negligible bending stiffness,[31] the biaxial strain produced at the center of the device can be written as

$$\varepsilon = \sigma(\nu)\left(\frac{\delta}{a}\right)^2 \quad (1)$$

where $\sigma(\nu)$ is a numerical constant that depends only on Poisson's ratio ν (see Supporting Information). For MoS_2, we take the value of $\nu = 0.29$,[32] resulting in $\sigma = 0.709$. This model has been shown to accurately describe graphene membranes in this geometry.[33] We can therefore measure ε at each p_{int} by using an AFM to find δ and a, and by varying the magnitude of p_{int} we can take optical measurements of the band gap and Raman shifts over a range of known strains.

We first studied the effect of strain on the PL of CVD and mechanically exfoliated monolayer devices, and Figure 2a shows the PL spectra of a monolayer device over the range of 0−2% biaxial strain. We incrementally increased p_{int} up to ~0.75 MPa corresponding to a strain of ~2%, and at successive pressures a PL, Raman, and AFM measurement was taken. At higher p_{int}, the membranes begin to delaminate from the surface as the force from Δp overcomes the adhesion to the substrate,[33] which limits the maximum possible strain with $\Delta p > 0$ to ~2%. Membranes in this geometry may slide at the edge of the well under high pressure,[34] however we only present data for devices that show no evidence of significant sliding (Figure S4). For optical measurements we used a 532 nm laser with a spot size of ~1 μm in diameter. Our devices were 8 μm in diameter, allowing us to focus the laser spot only on the region of biaxial strain in the center of the device. We observed that the PL peak red-shifted with increasing strain and also rapidly decreased in intensity, consistent with previous work[11] and theoretical predictions[7] (Figure S5).

Each spectrum in Figure 2a contains peaks resulting from the decay of the neutrally charged A and B excitons at approximately 1.89 and 2.05 eV respectively,[13] which form when electrons are excited across the direct band gap at the K-point and are bound to holes in the spin-split A and B valence bands. There is also a third peak (A^-) centered at 1.86 eV[35] that results from the decay of negatively charged trions which form when additional conduction band electrons bind to A excitons. To determine how all three peaks were affected by strain, we fitted three Voigt functions to each of our PL spectra (Figure 2b inset) and plotted the peak position of the A^-, A, and B peaks in Figure 2b. We found there was no difference in the shift rate between exfoliated and CVD grown devices, and that all three peaks had an approximately equal peak shift rate of -99 ± 6 meV/% that agrees well with theoretical predictions of 105 meV/%.[9]

We also took a corresponding Raman spectrum at each p_{int}, so we can similarly find the shift rate of the Raman modes with strain (Figure 2c). The two characteristic peaks of unstrained MoS_2, relating to in-plane (E^1_{2g}) and out-of-plane (A_{1g}) vibrations, are found at 385 and 405 cm^{-1} respectively. By fitting a Voigt function to each mode, we found that the modes shifted linearly at a rate of -1.7 cm^{-1}/% for the A_{1g} and -5.2 cm^{-1}/% for the E^1_{2g}, which agrees well with theoretical predictions[37] and previous experiments.[26] The differences in these values to those found in hydrostatic pressure studies[36] (in

DOI: 10.1021/acs.nanolett.6b02615
Nano Lett. XXXX, XXX, XXX−XXX

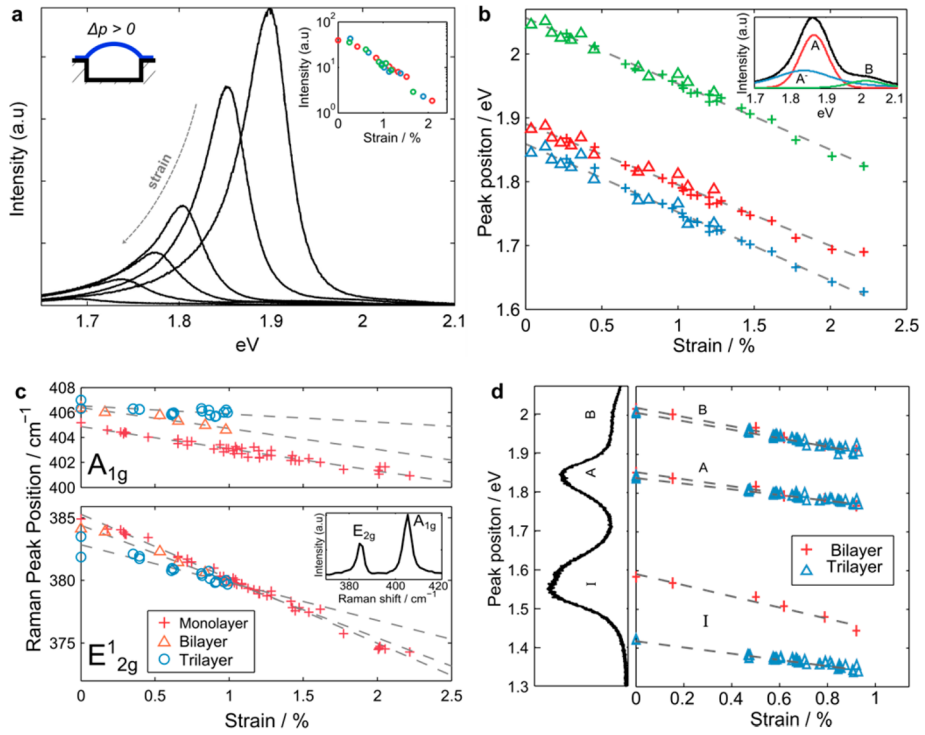

Figure 2. (a) The PL spectra for monolayer MoS_2 at different biaxial strains corresponding to different p_{inv}, and the relationship between strain and A peak intensity (inset). Intensities are normalized to the A_{1g} Raman peak. (b) The peak positions of the A (red), A^- (blue), and B (green) excitons as a function of biaxial strain for CVD (crosses) and exfoliated (triangles) monolayer devices. The peaks were fitted using three Voigt functions. (c) The E^1_{2g} and A_{1g} Raman modes for unstrained MoS_2 (inset) and peak positions as a function of biaxial strain for different membrane thicknesses. (d) A bilayer PL spectrum, and the peak positions of the A, B, and indirect I peak as a function of biaxial strain for exfoliated bilayer and trilayer devices.

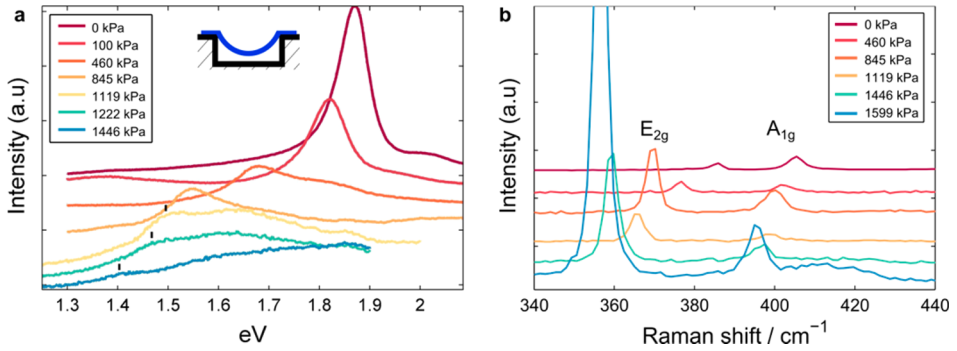

Figure 3. In situ measurements of (a) PL spectra for a monolayer device (scaled for comparison with ticks marking A peak position), with the largest pressure difference representing ~5% strain. (b) Raman spectra at increasing chamber pressures. Labels refer to the negative pressure difference $-\Delta p$ across the membrane, and Raman peaks are normalized to the silicon peak intensity.

which the A_{1g} mode has the higher shift rate) is likely due to the different type of deformation applied in the two cases. Using the formula[38] $\gamma = [\omega - \omega_0]/[2\varepsilon\omega_0]$, we determine the Grüneisen parameters for the modes to be $\gamma_{E^1_{2g}} = 0.68$ and $\gamma_{A_{1g}} = 0.21$, which are also in good agreement with the values found in earlier studies.[39,40] The position of the A_{1g} peak is known to vary with doping,[41] however as this is not the case with the more strain sensitive E^1_{2g} mode, its peak position can be used as a reliable way to measure the internal strain of monolayer MoS_2.

Multilayer MoS_2 is also a promising material for strain based applications,[20] so we used the same procedure to take strain and optical measurements of one bilayer device and five trilayer devices prepared by mechanical exfoliation. For these devices, we again observed Raman mode softening for both peaks (Figure 2c) but with smaller shift rates than were seen for monolayers (see Table S1 in Supporting Information). The PL spectrum of multilayer MoS_2 is distinguished from that of monolayers by the presence of a large additional peak resulting from indirect gap emission,[13] referred to as the I peak. The peak positions for the I, A, and B peaks are plotted against strain in Figure 2d. We determined the A peak shift rate to be −91 meV/% for bilayers and −73 meV/% for trilayers. The indirect I peak shifted considerably faster than the direct peaks in both bilayers and trilayers at a rate of −144 and −110 meV/% respectively.

To overcome the limitation in the magnitude of the applied strain imposed by delamination when $\Delta p > 0$, we can instead increase p_{ext} of the devices which deflects the membrane downward. To do this, the devices were placed in a custom-built pressure chamber with a sapphire window which allows

DOI: 10.1021/acs.nanolett.6b02615
Nano Lett. XXXX, XXX, XXX−XXX

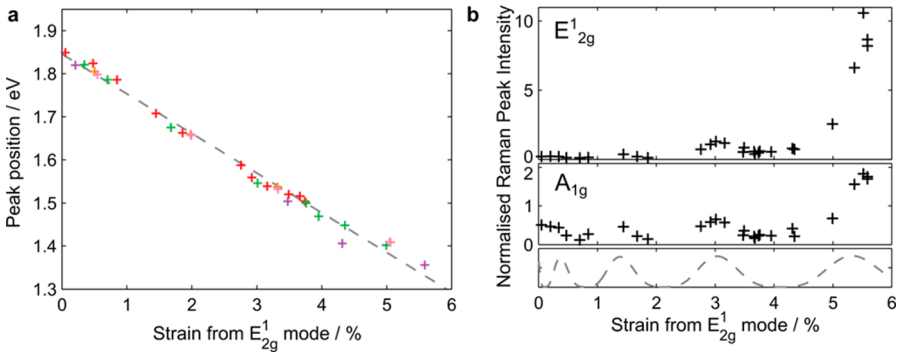

Figure 4. (a) The A peak position of the PL spectrum plotted against the strain as determined from the E^1_{2g} peak shift. In this case we fitted a single curve to the A peak feature, as the large decrease in PL intensity meant that the individual A and A^- peak contributions could not be resolved. Different colors represent different devices. (b) The integrated intensities of the E^1_{2g} and A_{1g} modes normalized to the silicon peak and plotted against strain. The expected intensity modulation due to interference is also plotted for comparison.

optical measurements to be taken at various p_{ext}.[35] The internal pressures of the cavities were $p_{int} = 0$, as the devices had been left to equilibrate in a vacuum chamber for several days prior to measurements. By pressurizing the chamber with N_2 gas, the greater $-\Delta p$ across the membrane deflects it further downward and produces an increased biaxial strain at the center of the device.

Figure 3a shows the PL spectrum as Δp is varied from 0 to −1.45 MPa. As before, the A peak redshifts with increasing strain and also rapidly decreases in intensity. The A peak intensity decreased faster than the B peak, so at the largest strains the peaks were of a comparable intensity. As determined from the energy shift of the A peak, we find that we can shift the band gap in this manner by as much as 500 meV.

At each p_{ext}, a Raman spectrum was also taken along with its corresponding PL spectrum. The data is normalized to the silicon peak and plotted in Figure 3b. We saw the softening of both modes with increasing strain as before and also observed the strain tuning of the second order 2LA(M) mode (Figure S7b). Because of the changing deflection of the bulge with pressure, the optical interference between light scattered off the membrane and light reflected off the silicon substrate is altered, which produces the oscillatory behavior in both the peak intensities with increasing pressure. As strains are increased, we observe a dramatic increase in the intensity of the E^1_{2g} mode relative to A_{1g} mode, which is an effect not reported in other studies.

Finally, by assuming the linear relationship we found earlier between the E^1_{2g} Raman mode and biaxial strain holds at the higher strains we are now considering, we use the position of the strain sensitive E^1_{2g} peak to determine the biaxial strain that was produced at each p_{ext} in Figure 3, and we can therefore determine the strain in our devices by optical measurements only.

The A peak position is plotted against this strain in Figure 4a, showing that biaxial strains as high as 5.6% can be achieved before membrane rupture. The relationship between the band gap shift and strain remains approximately linear at these high strains with a shift rate of 92 ± 6 meV/%, which is consistent with our earlier findings of 99 ± 6 meV/%.

We also plot the integrated intensities of both peaks (normalized to the silicon peak) against the strain as determined by the E^1_{2g} peak position (Figure 4b). At the highest strains, there was a 3-fold enhancement of the A_{1g} peak and more than a 20-fold enhancement of the E^1_{2g} peak. By using the Fresnel equations to model the effects of optical interference on our measurements due to the changing δ with pressure (Figure 4b bottom panel and Figure S6), we find that interference effects cannot explain these enhancements, nor the relative enhancement of E^1_{2g} over A_{1g}. We also rule out the changing curvature of our devices when strained as the source of this intensity increase (Figure S8).

Similar enhancements of the Raman peak intensities have been observed when laser excitation energies are resonant with an electronic transition.[42−44] Here, we maintain a constant laser energy of 2.33 eV, however as biaxial strain induces large changes to the electronic band structure, some transition energies may be moved closer to resonance with the laser excitation energy. We therefore attribute the increase in intensity of both peaks relative to the silicon peak to resonant Raman scattering resulting from the strain tuning of a higher level energy transition to be in resonance with the laser. A likely candidate for this transition is the C exciton at ∼2.8 eV,[43−45] because the redshift required to lower its energy to resonance with our laser would be ∼500 meV, which is a value consistent with the shift of the A peak at our highest strains. These results demonstrate not only that CVD grown monolayer MoS_2 films can withstand the remarkably high strains of 5.6% over micron-sized areas but that higher level optical transitions may also be tuned with strain.

The ability to continuously and reversibly modulate the optical band gap of monolayer MoS_2 by up to 25% allows significant control over the optical and electrical properties of the material, an effect that could be used to produce sensitive piezoresistive pressure sensors or broadband light absorbers. We also grew atomically thin membranes by CVD that are highly impermeable to gases and can withstand large pressure differences across them, suggesting that CVD grown MoS_2 could be promising as a gas separation membrane. The method used in this work may be extended to study the effects of biaxial strain on other 2D semiconducting materials and could also be used to determine the effects of very high strains on other strain dependent phenomena, such as magnetism,[46] chemical adsorption,[47] or piezoelectricity.[48]

■ ASSOCIATED CONTENT

Supporting Information

The Supporting Information is available free of charge on the ACS Publications website at DOI: 10.1021/acs.nanolett.6b02615.

DOI: 10.1021/acs.nanolett.6b02615
Nano Lett. XXXX, XXX, XXX−XXX

details of the growth and characterization of membranes, additional Raman shift rate data for multilayer samples, the procedure for device pressurization and optical measurements, gas permeance measurements, a discussion of the Hencky model, evidence of repeatability and the effects of membrane sliding, a comparison to theoretical work of the PL intensity decrease with strain, a discussion of interference effects with additional Raman mode data, and PL mapping data (PDF)

AUTHOR INFORMATION

Corresponding Author

*E-mail: bunch@bu.edu. Fax: 1-617-353-5866.

Notes

The authors declare no competing financial interest.

ACKNOWLEDGMENTS

This work was funded by the National Science Foundation (NSF), Grant 1054406 (CMMI: CAREER, Atomic Scale Defect Engineering in Graphene Membranes) and Grant 1411008, a grant to L.C. by the NSF Graduate Research Fellowship Program under Grant DGE-1247312, a grant to J.W.C. by the Department of Defense (DoD) Air Force Office of Scientific Research through a National Defense Science and Engineering Graduate (NDSEG) Fellowship, 32 CFR 168a, and a grant to B.L.K. by the Boston University Undergraduate Research Opportunities Program (UROP).

REFERENCES

(1) Li, J.; Shan, Z.; Ma, E. *MRS Bull.* **2014**, *39*, 108−114.
(2) Adams, A. R. *IEEE J. Sel. Top. Quantum Electron.* **2011**, *17* (5), 1364−1373.
(3) Sun, Y.; Thompson, S. E.; Nishida, T. *J. Appl. Phys.* **2007**, *101*, 104503.
(4) Zhu, T.; Li, J. *Prog. Mater. Sci.* **2010**, *55* (7), 710−757.
(5) Lugstein, A.; Steinmair, M.; Steiger, A.; Kosina, H.; Bertagnolli, E. *Nano Lett.* **2010**, *10*, 3204−3208.
(6) Li, T. *Phys. Rev. B - Condens. Matter Mater. Phys.* **2012**, *85* (23), 1−5.
(7) Steinhoff, A.; Kim, J. H.; Jahnke, F.; Rösner, M.; Kim, D. S.; Lee, C.; Han, G. H.; Jeong, M. S.; Wehling, T. O.; Gies, C. *Nano Lett.* **2015**, *15* (10), 6841−6847.
(8) He, K.; Poole, C.; Mak, K. F.; Shan, J. *Nano Lett.* **2013**, *13* (6), 2931−2936.
(9) Plechinger, G.; Castellanos-Gomez, A.; Buscema, M.; van der Zant, H. S. J.; Steele, G. a; Kuc, A.; Heine, T.; Schüller, C.; Korn, T. *2D Mater.* **2015**, *2* (1), 015006.
(10) Castellanos-Gomez, A.; Roldan, R.; Cappelluti, E.; Buscema, M.; Guinea, F.; Van Der Zant, H. S. J.; Steele, G. A. *Nano Lett.* **2013**, *13* (11), 5361−5366.
(11) Conley, H. J.; Wang, B.; Ziegler, J. I.; Haglund, R. F.; Pantelides, S. T.; Bolotin, K. I. *Nano Lett.* **2013**, *13* (8), 3626−3630.
(12) Hui, Y. Y.; Liu, X.; Jie, W.; Chan, N. Y.; Hao, J.; Hsu, Y.-T.; Li, L.-J.; Guo, W.; Lau, S. P. *ACS Nano* **2013**, *7* (8), 7126−7131.
(13) Mak, K. F.; Lee, C.; Hone, J.; Shan, J.; Heinz, T. F. *Phys. Rev. Lett.* **2010**, *105* (13), 2−5.
(14) Radisavljevic, B.; Radenovic, A.; Brivio, J.; Giacometti, V.; Kis, A. *Nat. Nanotechnol.* **2011**, *6*, 147−150.
(15) Tsai, M. L.; Su, S. H.; Chang, J. K.; Tsai, D. S.; Chen, C. H.; Wu, C. I.; Li, L. J.; Chen, L. J.; He, J. H. *ACS Nano* **2014**, *8* (8), 8317−8322.
(16) Lee, H. S.; Min, S. W.; Chang, Y. G.; Park, M. K.; Nam, T.; Kim, H.; Kim, J. H.; Ryu, S.; Im, S. *Nano Lett.* **2012**, *12* (7), 3695−3700.
(17) Bertolazzi, S.; Brivio, J.; Kis, A. *ACS Nano* **2011**, *5* (12), 9703−9709.
(18) Scalise, E.; Houssa, M.; Pourtois, G.; Afanas'ev, V.; Stesmans, A. *Nano Res.* **2012**, *5* (1), 43−48.
(19) Peelaers, H.; Van De Walle, C. G. *Phys. Rev. B: Condens. Matter Mater. Phys.* **2012**, *86* (24), 1−5.
(20) Manzeli, S.; Allain, A.; Ghadimi, A.; Kis, A. *Nano Lett.* **2015**, *15* (8), 5330−5335.
(21) Yu, S.; Xiong, H. D.; Eshun, K.; Yuan, H.; Li, Q. *Appl. Surf. Sci.* **2015**, *325*, 27−32.
(22) Feng, J.; Qian, X.; Huang, C.; Li, J. *Nat. Photonics* **2012**, *6* (12), 866−872.
(23) Roldan, R.; Castellanos-gomez, A.; Cappelluti, E. *J. Phys.: Condens. Matter* **2015**, *27*, 313201.
(24) Nayak, A. P.; Bhattacharyya, S.; Zhu, J.; Liu, J.; Wu, X.; Pandey, T.; Jin, C.; Singh, A. K.; Akinwande, D.; Lin, J.-F. *Nat. Commun.* **2014**, *5* (3731), 1−9.
(25) Wang, Y.; Cong, C.; Yang, W.; Shang, J.; Peimyoo, N.; Chen, Y.; Kang, J.; Wang, J.; Huang, W.; Yu, T. *Nano Res.* **2015**, *8* (8), 2562−2572.
(26) Li, H.; Contryman, A. W.; Qian, X.; Ardakani, S. M.; Gong, Y.; Wang, X.; Weisse, J. M.; Lee, C. H.; Zhao, J.; Ajayan, P. M.; Li, J.; Manoharan, H. C.; Zheng, X. *Nat. Commun.* **2015**, *6*, 7381.
(27) Nayak, A. P.; Pandey, T.; Voiry, D.; Liu, J.; Moran, S. T.; Sharma, A.; Tan, C.; Chen, C. H.; Li, L. J.; Chhowalla, M.; Lin, J. F.; Singh, A. K.; Akinwande, D. *Nano Lett.* **2015**, *15* (1), 346−353.
(28) Signorello, G.; Karg, S.; Björk, M. T.; Gotsmann, B.; Riel, H. *Nano Lett.* **2013**, *13* (3), 917−924.
(29) Bunch, J. S.; Verbridge, S. S.; Alden, J. S.; Van Der Zande, A. M.; Parpia, J. M.; Craighead, H. G.; McEuen, P. L. *Nano Lett.* **2008**, *8* (8), 2458−2462.
(30) Suk, J. W.; Kitt, A.; Magnuson, C. W.; Hao, Y.; Ahmed, S.; An, J.; Swan, A. K.; Goldberg, B. B.; Ruoff, R. S. *ACS Nano* **2011**, *5* (9), 6916−6924.
(31) Fichter, W. *NASA Technol. Pap.* **1997**, *3658*, 1−24.
(32) Cooper, R. C.; Lee, C.; Marianetti, C. a.; Wei, X.; Hone, J.; Kysar, J. W. *Phys. Rev. B: Condens. Matter Mater. Phys.* **2013**, *87* (3), 035423.
(33) Koenig, S. P.; Boddeti, N. G.; Dunn, M. L.; Bunch, J. S. *Nat. Nanotechnol.* **2011**, *6* (9), 543−546.
(34) Kitt, A. L.; Qi, Z.; Remi, S.; Park, H. S.; Swan, A. K.; Goldberg, B. B. *Nano Lett.* **2013**, *13*, 2605−2610.
(35) Mak, K. F.; He, K.; Lee, C.; Lee, G. H.; Hone, J.; Heinz, T. F.; Shan, J. *Nat. Mater.* **2012**, *12* (3), 207−211.
(36) Scheuschner, N.; Ochedowski, O.; Kaulitz, A. M.; Gillen, R.; Schleberger, M.; Maultzsch, J. *Phys. Rev. B: Condens. Matter Mater. Phys.* **2014**, *89* (12), 2−7.
(37) Bandaru, N.; Kumar, R. S.; Sneed, D.; Tschauner, O.; Baker, J.; Antonio, D.; Luo, S.-N.; Hartmann, T.; Zhao, Y.; Venkat, R. *J. Phys. Chem. C* **2014**, *118* (6), 3230−3235.
(38) Zabel, J.; Nair, R. R.; Ott, A.; Georgiou, T.; Geim, A. K.; Novoselov, K. S.; Casiraghi, C. *Nano Lett.* **2012**, *12* (2), 617−621.
(39) Wang, Y.; Cong, C.; Qiu, C.; Yu, T. *Small* **2013**, *9* (17), 2857−2861.
(40) Rice, C.; Young, R. J.; Zan, R.; Bangert, U.; Wolverson, D.; Georgiou, T.; Jalil, R.; Novoselov, K. S. *Phys. Rev. B: Condens. Matter Mater. Phys.* **2013**, *87* (8), 1−5.
(41) Chakraborty, B.; Bera, A.; Muthu, D. V. S.; Bhowmick, S.; Waghmare, U. V.; Sood, A. K. *Phys. Rev. B: Condens. Matter Mater. Phys.* **2012**, *85* (16), 2−5.
(42) Liu, H.-L.; Guo, H.; Yang, T.; Zhang, Z.; Kumamoto, Y.; Shen, C.-C.; Hsu, Y.-T.; Li, L.-J.; Saito, R.; Kawata, S. *Phys. Chem. Chem. Phys.* **2015**, *17* (22), 14561−14568.
(43) Carvalho, B. R.; Malard, L. M.; Alves, J. M.; Fantini, C.; Pimenta, M. A. *Phys. Rev. Lett.* **2015**, *114* (13), 1−5.
(44) Carvalho, B. R.; Malard, L. M.; Alves, J. M.; Fantini, C.; Pimenta, M. A. *Phys. Rev. Lett.* **2016**, *116* (8), 089904.
(45) Yu, Y.; Yu, Y.; Cai, Y.; Li, W.; Gurarslan, A.; Peelaers, H.; Aspnes, D. E.; Van de Walle, C. G.; Nguyen, N. V.; Zhang, Y.-W.; Cao, L. *Sci. Rep.* **2015**, *5*, 16996.

DOI: 10.1021/acs.nanolett.6b02615
Nano Lett. XXXX, XXX, XXX−XXX

(46) Manchanda, P.; Sharma, V.; Yu, H.; Sellmyer, D. J.; Skomski, R. *Appl. Phys. Lett.* **2015**, *107*, 032402.
(47) Kou, L.; Du, A.; Chen, C.; Frauenheim, T. *Nanoscale* **2014**, *6*, 5156−5161.
(48) Wu, W.; Wang, L.; Li, Y.; Zhang, F.; Lin, L.; Niu, S.; Chenet, D.; Zhang, X.; Hao, Y.; Heinz, T. F.; Hone, J.; Wang, Z. L. *Nature* **2014**, *514* (7523), 470−474.

DOI: 10.1021/acs.nanolett.6b02615
Nano Lett. XXXX, XXX, XXX−XXX